

An experimental study of boundary-layer transition over a rotating, compliant disk

A. J. Colley, P. J. Thomas,^{a)} P. W. Carpenter, and A. J. Cooper^{b)}

Fluid Dynamics Research Centre, School of Engineering, University of Warwick, Coventry, CV4 7AL, United Kingdom

(Received 11 March 1999; accepted 9 July 1999)

An experimental study is described which investigates the laminar-turbulent transition of the boundary layer over rigid and compliant disks rotating under water. Hot-film data are presented and analyzed to produce neutral-stability curves. It appears to be the first time that such data has become available for a compliant disk. Our experiments employing a rigid disk essentially confirm the results of previous authors. For the flow over the compliant disk the turbulence levels in the transitional and fully turbulent flow regimes are found to be considerably lower than the corresponding levels for the rigid disk. The analysis of our experimental data suggests that wall compliance has a stabilizing influence in the frequency range associated with the Type I cross-flow instability. Nevertheless, compliance is found to have an overall destabilizing effect on the boundary-layer flow. This results in a substantially lower transitional Reynolds number compared to the case of the rigid disk. The experimental observations are in qualitative agreement with our theoretical predictions. It is argued that the reduced transitional Reynolds number for the compliant disk might indicate that transition for such a disk results from a convective-instability mechanism and not from an absolute-instability mechanism as has recently been suggested in the literature to be the case for a rigid disk. © 1999 American Institute of Physics. [S1070-6631(99)00111-7]

I. INTRODUCTION

For over 5 decades the rotating-disk flow has provided the paradigm for the study of laminar-turbulent transition in three-dimensional (3D) boundary-layer flows. The study of this flow has made major contributions to our knowledge of the flow physics associated with the transition process. A relatively recent review of the research related to the rotating disk flow can be found in Reed and Saric.¹ A detailed account of the most recent research results is contained in the introduction of one of our own papers.² The reader is referred to these publications for a comprehensive overview of the subject. We will restrict ourselves here to a very brief introduction.

The rotating-disk flow is appealing to both experimentalists and theoreticians alike. For experimentalists it represents a relatively easily accessible and low-noise environment for making detailed measurements if compared with wind tunnels or water channels. Its attraction for theoreticians results from the existence of a similarity solution first derived by Kármán³ which is an exact solution of the Navier–Stokes equations. From a more applied viewpoint the relevance of the rotating-disk flow is that the transition process exhibits many of the features displayed by the fully 3D boundary layers found in many engineering applications. A good example is, for instance, the boundary layer over a highly swept wing. This flow and also that over the rotating

disk both display the typical cross-flow vortices resulting from the inviscid-instability mechanism associated with an inflexion point in the boundary-layer velocity profile. In the context of the rotating-disk flow this instability mode is referred to as the Type I instability (or as Class B in some older publications). It leads to the well-known spiral vortices characterizing the laminar-turbulent transition region which separates the laminar flow regime in the disk's center from the fully turbulent flow located further radially outward. For flow visualizations showing the spiral vortices refer, for instance, to the classic paper by Gregory, Stuart, and Walker⁴ or to the review article by Reed and Saric.¹

It has been known for many years^{5–10} that wall compliance can postpone transition for the essentially 2D boundary layer over a flat plate. In fact, it has been established theoretically that Tollmien–Schlichting waves can be suppressed completely for a sufficiently high level of compliance.⁸ Physically the stabilizing mechanism is a combination of a reduced rate of Reynolds stress production and enhanced dissipation rates. Cooper and Carpenter² have recently shown theoretically that much the same holds for the Type I cross-flow instability over the compliant rotating disk. Both Tollmien–Schlichting waves and the Type I instability are examples of negative-energy waves (Class A in the terminology of Landahl⁷ and Benjamin⁶ who first introduced the concept), i.e., dissipative processes in the compliant wall tend to have a destabilizing effect. For the compliant wall on a flat plate hydroelastic instabilities in the form of traveling-wave flutter and divergence can set in when the level of compliance is too great. Traveling-wave flutter is an example of a positive-energy wave (Class B in the original

^{a)} Author to whom correspondence should be addressed. Electronic mail: pjt@eng.warwick.ac.uk

^{b)} DAMTP, University of Cambridge, Silver Street, Cambridge, CB3 9EW, United Kingdom

terminology^{6,7}) which is stabilized by dissipative effects in the compliant wall. Divergence is an absolute instability. Similar hydroelastic instabilities can also occur for the rotating compliant disk. But, in addition, other linear eigenmodes exist for the rigid disk, which can be modified by wall compliance. The effect of wall compliance on the viscous Type II instability appears to be rather complex and the theory suggests that it is a positive energy wave.² Yet another linear eigenmode (Type III) is found for the rotating disk and, as shown recently by Lingwood,^{11,12} this can coalesce with the Type I to form an absolute instability. Cooper and Carpenter¹³ have shown theoretically that wall compliance has a strong stabilizing effect on this absolute instability.

Whereas previous studies^{5–10} have focused on 2D boundary layers the present study of the rotating-disk flow is the first to investigate the influence of wall compliance on transition in fully 3D boundary layers. The only studies known to us which previously considered a rotating disk covered with a compliant coating are due to Hansen and Hunston,^{14–16} Chung,¹⁷ and very recently Fitzgerald *et al.*^{18,19} All these studies only focused on torque measurements. They did not investigate the transition process or the details of the flow as such. The compliant disks studied by Chung¹⁷ were of a relatively complex structure. For some of the walls tested a torque reduction was observed which implies drag-reducing capability and transition delay. Fitzgerald *et al.* have used a polymer gel-foam composite as the compliant material for their disks. This material was developed to have viscoelastic properties close to those measured for live dolphin blubber. Fitzgerald *et al.* also report a reduced torque for their compliant discs compared with a rigid-disk control. Transition, as evidenced by a sharp change in slope of the curve displaying torque vs disk rotation speed, was also postponed to higher Reynolds number over these discs coated with the polymer gel-foam. The flow physics responsible for these torque reductions was, however, not revealed.

Hansen and Hunston^{14–16} carried out torque measurements for a rotating disk in water in connection with an observed hydroelastic instability developing on the disk surface. This instability leads to a wave structure on the surface when it is sufficiently compliant. Hansen and Hunston¹⁴ report that wall compliance does not appear to affect the flow in any measurable way as long as the compliance remains below a certain critical level. It will be seen that our study strongly contravenes this earlier observation.

Although we did use a different material than Hansen and Hunston^{14–16} our compliant walls have a similar simple structure and consist of a single homogeneous viscoelastic layer. We work, however, with compliant discs which are significantly *less compliant* than the critical level stated by Hansen and Hunston. In fact, we originally chose such a comparatively stiff compliant wall with the aim of using this disk, rather than a completely rigid disk, as a control for comparison with experiments on much more compliant disks manufactured from the same type of material (i.e., silicone rubber). For the stiff compliant walls we anticipated that there would be little change in the stability characteristics and the transition processes in comparison to the correspond-

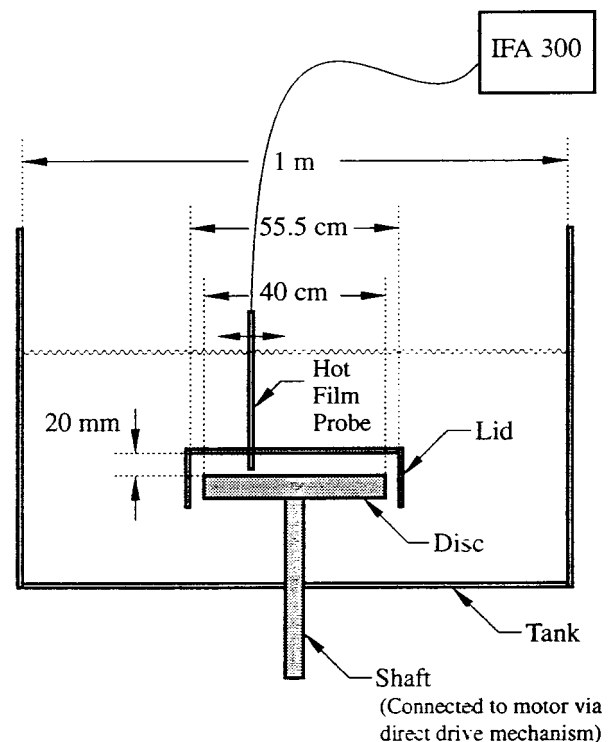


FIG. 1. Sketch of the rotating disk facility.

ing flow over the completely rigid disc. Surprisingly our experiments revealed that this is not so. Even relatively stiff compliant discs were found to exhibit markedly different stability characteristics and transition processes than the rigid disc.

II. EXPERIMENTAL SETUP AND TECHNIQUES

The rotating-disk facility developed for the present study is schematically illustrated in Fig. 1. It is, in principle, very similar to facilities used previously elsewhere. It consists of a disc with a radius of $R=200$ mm spinning under water around a vertical axis of rotation. The rotational velocity of the disc is $\Omega=2\pi f_D$, with f_D being the disc's rotational frequency in Hertz. The boundary-layer thickness δ over the disc is defined to be that height where the azimuthal flow velocity v_ϕ has the value $v_\phi=0.01\Omega r$, where r is the radial distance from the disc's center. According to Kármán's³ similarity solution the boundary-layer thickness is then given by (see also Owen and Rogers²⁰)

$$\delta=5.5\left(\frac{\nu}{\Omega}\right)^{1/2}, \quad (1)$$

where ν is the kinematic viscosity of water.

The disc is mounted inside a large tank with a diameter of 1 m and a height of 650 mm. A circular lid (diameter 555 mm) is placed over the rotating disc, as illustrated in Fig. 1. This is similar to the arrangement used by Jarre, Le Gal, and Chauve.^{21–23} The lid is rigidly mounted at a height $h=20$ mm above the disc surface. In terms of the boundary-layer thickness this corresponds to $h\approx 10\delta$ for the experiments described here.

The lid was incorporated in our experimental setup essentially for two reasons. First, it enables us to directly compare our own results with the data of Jarre *et al.*^{21–23} Such a comparison facilitates, in particular, the verification of the suitability of our experimental equipment. As far as we know the results of Jarre *et al.* represent the only available data of boundary-layer transition over a rigid disk spinning under water. Second, without the lid being in place the entire fluid inside the tank is spun up while the disk is rotating. The resulting deformation of the free surface and the interaction of the rotating fluid with supports for the measurement equipment has proven to be detrimental to the experiment. The measurement environment is significantly improved if the lid is in place; this is reflected by much cleaner data being obtained. The lid does, of course, result in a modified flow field in comparison to the flow established by a disk spinning in an infinite medium. The differences between the two types of flow are discussed in detail for instance in Owen and Rogers²⁰ or Wimmer.²⁴ In the present context the most critical difference between the restricted and the unrestricted flow is, probably, that for the enclosed-disk geometry there exists the possibility of velocity fluctuations being recirculated into the boundary layer by the large-scale mean flow associated with the restricted flow geometry. However, our experimental results will show that this recirculation did, apparently, not lead to any measurable influences on the aspects of the transition process which are considered here.

The top of the lid accommodates a radially orientated narrow slot through which a hot-film probe can access the measuring region. The slot extends over the entire disk radius and the hot-film probe can be moved to any radial location over the disk surface. The traversing of the hot-film probe is fully computer controlled in both the radial and the vertical direction. The mechanical components of the traverse mechanism and the probe support are designed around a two-axis linear-motor system (omitted from Fig. 1 for clarity) mounted above the water tank.

We used a TSI IFA 300 constant-temperature hot-film anemometry system for our study. All measurements were carried out with a single-sensor hot-film boundary-layer probe. Acquisition of hot-film data was triggered by an optoelectronic detection of a reference timing mark on the shaft connected to the motor driving the disk. When the lid was removed from the tank the probe could be traversed across the whole diameter of the water tank. By moving the probe through the tank at a number of specified constant velocities it could, thus, be calibrated within the actual measuring environment inside the water tank.

For the measurement of the radial velocity component v_r , the sensor of the probe was aligned parallel to the disk surface and at a right angle to the disk radius. Correspondingly, the sensor was orientated radially for the measurement of the azimuthal velocity component v_ϕ . The actual total flow velocity is a superposition of the radial and the azimuthal flow component. Consequently the sensor is, in both its measuring alignments, yawed with respect to the total flow velocity. This leads to a biasing of the measured velocity data owing to effective along-sensor cooling.²⁵ The radial flow velocity does not change linearly with the azimuthal flow component

for varying probe heights above the disk surface. Consequently the effective yaw angle also changes with the height of the probe. In previous studies^{12,21–23,26} the yaw-angle bias was explicitly or implicitly assumed to be negligible and this assumption was made without a proper verification of its validity. We have experimentally determined an estimate for the magnitude of the biasing of the velocity data. To this end we have traversed the probe through the fluid with the sensor mounted at three different yaw angles to the actual direction of the motion. This yields three different correction factors. Each factor quantifies the yaw angle bias at one particular probe height above the disk. We have not determined yaw-angle correction factors for a larger number of yaw angles as the principal results obtained from our data analysis are not affected by the yaw-angle bias. Where it is appropriate we will, nevertheless, comment on how the yaw-angle bias has influenced our measured velocity data.

Filtered tap water was used for the experiments. The filtering system removes particles larger than $0.4 \mu\text{m}$ in diameter. The experiments were performed at water temperatures of 19°C . The laboratory in which the experimental facility is located is air-conditioned; the air temperature was kept constant to within $\pm 2.0^\circ\text{C}$. By monitoring the water temperature over several weeks we established that the largest temperature fluctuations observed were, in fact, smaller than $\pm 0.5^\circ\text{C}$.

Compliant coatings were manufactured from room-temperature vulcanizing silicone rubber. The rubber was modified by the addition of 10% (by weight) of 20 cSt ($20 \text{ mm}^2/\text{s}$) silicone oil. The process for manufacturing a coating is, in principle, to pour the liquid rubber onto a disk mold with a 10 mm high peripheral rim. The disk was then covered with a smooth glass plate, flipped over and the silicone rubber was allowed to cure. Flipping over the disk ensured that any air entrapped between the glass plate and the liquid silicone rubber would rise. Entrapped bubbles, thus, move away from what would constitute the actual compliant surface once the silicone had cured and the glass plate was removed. Flipping the disk over, thus, ensures that a smooth compliant surface is obtained which is free of surface dents resulting from air entrapment. It is emphasized that it required many trials to perfect the manufacturing process in order to give a smooth compliant coating which was free of ripples or dents. The first experiments on the compliant disk were performed seven days after the disk had been manufactured. The actual working surface for the rigid-disk experiments is a circular glass plate mounted on an appropriate substructure. A glass plate was chosen as it provides a smoother, more resistant and noncorrosive surface than a metallic surface.

The surface roughness of the compliant and rigid disks were measured on a standard Rank–Taylor–Hobson Taly-surf facility. The suitability of this technique for evaluating the surface roughness of compliant materials is discussed in Thomas *et al.*²⁷ The roughness height of the rigid glass disk was found to be $h_r = 0.007 \pm 0.003 \mu\text{m}$ and the corresponding height of the compliant disc was $h_c = 0.313 \pm 0.08 \mu\text{m}$. In terms of the boundary-layer thickness this corresponds to $h_r \approx 3.6 \times 10^{-6} \delta$ and $h_c \approx 1.6 \times 10^{-4} \delta$.

The elastic properties of the compliant material are characterized in terms of its modulus of elasticity E . We have developed a precision apparatus for measuring the modulus of elasticity of compliant coatings *in situ*, i.e., while the coatings are attached to the disk. The principle of operation of this facility is to press a small spherically-shaped indenter (radius, $r_i = 5$ mm) onto the surface of the compliant material. The indentation depth δ_i is measured as a function of the restitutive force N . The modulus of elasticity can then be determined according to classic Hertzian theory²⁸ from the expression

$$\delta_i = \left(\frac{9N^2}{16E^2 r_i} \right)^{1/3}. \quad (2)$$

Following two days of undisturbed curing of the silicone rubber in the disk mold we have measured a value of $E = 380$ kPa for the compliant coating. However, the silicone rubber is subject to an aging process which affects its level of compliance. Four months after completing the first set of experiments we have repeated the experimental program. By then the silicone rubber had become more compliant and the modulus of elasticity had fallen to $E = 333$ kPa. Following this second set of experiments we left the disk continuously immersed under water for one week upon which we repeated the experimental program once more. For this third set of experiments we measured a value of $E = 290$ kPa. The dependence of the modulus of elasticity on the age of the silicone rubber and external factors influencing it evidently imposes constraints on the repeatability of otherwise identical experimental runs.

For compliant walls of a similar type to ours Hansen and Hunston¹⁴ found that the critical flow speed v_c for the onset of hydroelastic instability is given by

$$v_c = 1.41 \sqrt{\frac{G}{\rho_L}}, \quad (3)$$

where G and ρ_L are, respectively, the modulus of rigidity of the compliant material and the density of the flowing liquid. For almost incompressible materials like silicone rubber, $E \approx 3G$. With the values of the modulus of elasticity determined above and for a density of $\rho_L \approx 1000$ kg/m³ for water one obtains from Eq. (3) a value of $v_c \approx 14$ – 16 m/s. For the present experiment the rotation rate was equal to $\Omega = 7.85$ rad/s and the largest linear velocity, at the edge of the disk, is thus 1.57 m/s. This velocity is sufficiently small to be confident that the hydroelastic instability was not excited in our experiment.

We have also determined an estimate for the damping coefficient associated with the viscoelastic properties of the silicone rubber. For this we adopted a simple technique whereby a small metal sphere (radius, 5 mm) was dropped on the compliant surface from a height h_0 . The rebound height h_1 , following the first impact of the sphere with the compliant surface, was then measured. This enables an evaluation of the fraction of the energy dissipated by the silicone rubber during the impact. By means of this method

we obtained a value of $\ln(h_0/h_1) \approx 1.23 \pm 0.06$. This estimate was obtained when the compliant coating had an elastic modulus of $E = 333$ kPa.

In order to have some control over the onset of the boundary-layer transition we adopted the technique used by other researchers (for example, Jarre *et al.*,²³ Wilkinson and Malik²⁶) in the past. These authors generated small disturbances within the boundary layer by means of a small roughness element attached to the disk surface. Transition does, of course, also occur in the absence of such a roughness element. Initial test runs during the early stages of our experimental program were, in fact, carried out on a disk without a roughness element. These runs revealed, however, that for constant Reynolds numbers evidence of transition as characterized by the development of spiral vortices tended to appear and disappear at randomly varying locations within successively sampled hot-film signals. When a roughness element is attached to the disk first evidence of transition always appears at a well-defined constant position within the signals. In order to facilitate comparisons of our own data with the data of previous authors we have, consequently, adopted their approach to study the case when transition is triggered by a roughness element.

The roughness element consisted of a small (1 mm \times 1 mm) piece of adhesive polyester tape. The tape was approximately 0.1 mm thick and, thus, protruded into the boundary layer to a height of approximately 0.05δ . The dimensions of the roughness element were the same for the experiments with the rigid and the compliant disk such that the type and the magnitude of the disturbances generated were also the same. The particular dimensions of the roughness element were chosen in order to produce disturbances which can be assumed to be of comparable magnitude to those generated in the study of Wilkinson and Malik.²⁶

III. EXPERIMENTAL RESULTS

For the discussion of the experimental results it is necessary to introduce the following conventional nomenclature. The Reynolds number Re associated with the rotating disk flow is defined as

$$Re = \frac{r}{\delta^*}, \quad (4)$$

where r is the radial distance from the center of the disk and δ^* is given by

$$\delta^* = \sqrt{\frac{\nu}{\Omega}}. \quad (5)$$

With respect to Kármán's³ similarity solution δ^* corresponds to that height over the disk where the azimuthal component of the flow velocity equals $v_\phi = 0.5 \Omega r$.

The vertical height z over the disk is nondimensionalized according to

$$\zeta = \frac{z}{\delta^*}. \quad (6)$$

The radial component v_r and the azimuthal component v_ϕ of the flow velocity in the boundary layer are expressed in non-dimensional form as

$$F(\zeta) = \frac{v_r}{\Omega r}; \quad (7a)$$

$$G(\zeta) = \frac{v_\phi}{\Omega r} \quad (7b)$$

The theoretical values for $F(\zeta)$ and $G(\zeta)$ according to Kármán³ can be found in tabulated form for instance in Owen and Rogers.²⁰

In the following sections we will initially establish that our experimental procedures are adequate and that our collected data are sufficiently accurate to reproduce the results of other authors for the boundary-layer flow over a rigid disk. We will then present corresponding results for the flow over a compliant disk and compare them to the rigid-disk data.

A. Boundary-layer profiles for mean flow velocity

A rotating disk which is covered by a stationary lid gives rise to the development of a Batchelor-type flow^{20,24,29} in the enclosed fluid-filled space between the disk and the lid. This flow is characterized by boundary layers on both the rotating disk as well as the stationary lid. Between the disk and the lid a core of fluid rotates with a constant angular velocity ω . The flow over the rotating disk is, thus, analogous to the case of the flow over a disk spinning in a rotating fluid. Batchelor-type velocity profiles were for instance computed numerically by Rogers and Lance³⁰ or Dijkstra and van Heijst³¹ for various experimental conditions. Immediately above the rotating disk these velocity profiles represent modified versions of the similarity solutions obtained by Kármán³ for a rotating, free disk for which the flow velocity far from the disk is zero.

Our experimental data points for the velocity components of the flow velocity over the rigid disk are compared with theoretical velocity profiles in Figs. 2(a) and 2(b). The dotted lines represent the similarity solution for a free disk after Kármán. The solid lines display a Batchelor-type profile computed by Rogers and Lance³⁰ for $\omega/\Omega=0.2$ and were taken off Fig. 3.4(a) of Owen and Rogers.²⁰ Our data points in Fig. 2(b) suggest that $G(\zeta)$ approaches a value between $0.1 < \omega/\Omega < 0.2$ for larger ζ . Hence, the actual velocity profile for the flow established in the present experiment should be located between the two theoretical curves shown in Figs. 2(a) and 2(b).

The experimental data displayed in the two figures are the velocity values as obtained from the anemometer. As discussed in Sec. II these data are subject to a yaw-angle bias. We have determined estimates for this bias at three different heights above the disk. Due to the yaw-angle bias the radial velocity component is measured approximately 20% too high for heights $1 \leq \zeta \leq 3$; this error decreases to about 10% at $\zeta=8$. Correspondingly the azimuthal component of the flow velocity is measured approximately 1% too high for $1 \leq \zeta \leq 3$ and the error increases to about 5% at $\zeta=8$.

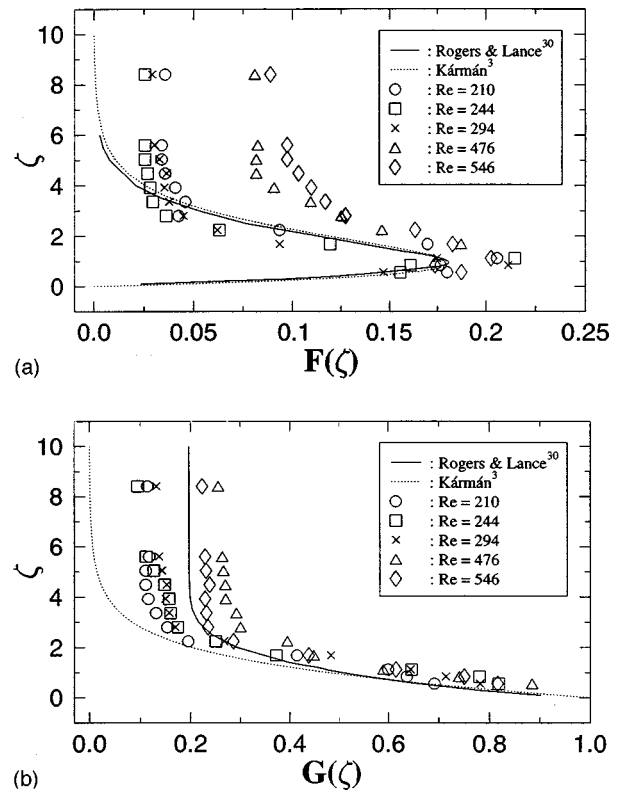


FIG. 2. Comparison of the measured mean flow velocity within the boundary layer with the similarity solution derived by Kármán (Ref. 3) and with the Batchelor-type profiles of Rogers and Lance (Ref. 30). (a) Radial velocity component, (b) azimuthal flow component.

We have not applied yaw-angle corrections to the data points displayed in Figs. 2(a) and 2(b). This would have required an interpolation between the three measured correction factors in order to obtain such factors at heights ζ where the yaw-angle bias was not determined experimentally. This, however, would have effectively resulted in a distortion of the velocity profiles and would not have revealed any further information of relevance to the actual goal of this study.

In any case, Figs. 2(a) and 2(b) show that our data reveal a satisfactory agreement with the expected theoretical velocity profiles. Our Figs. 2(a) and 2(b) are similar to the corresponding Figs. 4(a)–4(c) of Lingwood¹² and Fig. 7(a) of Jarre *et al.*²² This shows that we are capable of resolving the mean boundary-layer flow with an accuracy comparable to that achieved in previous studies. In the remainder we will analyze the experimental velocity signals in terms of their Fourier components only. Consequently, the yaw-angle bias does not need to be taken into account any further. In fact it would probably be permissible to carry out the experiments with an uncalibrated hot-film probe as has indeed been done by Jarre *et al.*

B. Qualitative development of hot-film signals

Figures 3(a) and 3(b) display samples of raw data signals of the azimuthal component of the flow velocity as measured with our hot-film probe. The scale of the y-axis for the displayed data samples is arbitrary and varies between different signals. The sole purpose of Figs. 3(a) and 3(b) is to document and compare the qualitative changes associated with

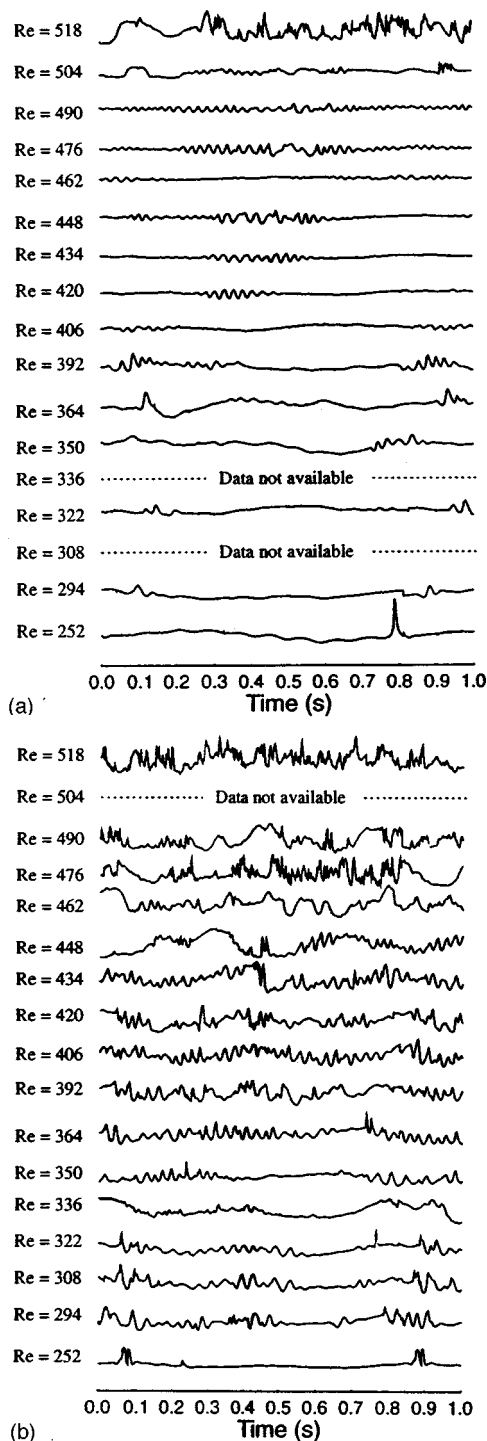


FIG. 3. Comparison of raw velocity signals obtained for the azimuthal component of the flow velocity over a (a) rigid disk and (b) compliant disk ($\Omega=7.85$ rad/s, $\zeta=1.29$).

the nature of the probe signal for the rigid and the compliant disk when the Reynolds number is increased. Figure 3(a) shows signals obtained for a rigid disk and Fig. 3(b) displays the corresponding data for a compliant disk. Each sample signal of length 1 s corresponds to 1.25 disk revolutions. All displayed signals were collected at a dimensionless height of $\zeta=1.29$ above the disk.

The signal obtained for the rigid disk at $Re=252$ which is displayed in Fig. 3(a) shows an almost constant flow ve-

locity over the entire time interval apart from a narrow peak at $t \approx 0.79$ s. This peak corresponds to the disturbance introduced in the flow by the presence of the roughness element attached to the disk surface. The roughness element is positioned at $Re=249$ and it is thus located approximately 1 mm radially inwards from the position corresponding to $Re=252$. We have observed that the elevation of the disturbance peak over the mean signal varies with the height of the hot-film probe over the disk. For the azimuthal flow component at $Re=252$ the peak elevation lies in the range between 20% and 10% of the mean flow velocity for probe heights ζ between 2.41 and 0.45.

For $Re=294$ the initially narrow disturbance peak introduced by the roughness element has somewhat dispersed and it has traveled to the right on the time axis where it is now located around the position $t \approx 0.85$ s. Accordingly the dispersed disturbance associated with a preceding disk revolution has entered the viewing window and can also be seen on the signal trace located around $t \approx 0.1$ s. This process is also very nicely illustrated by Fig. 5 of Lingwood¹² where a larger number of signals are depicted—the reader is encouraged to refer to this figure. Our Fig. 3(a) shows that by $Re=420$ a clear wave packet is visible on the velocity-time trace. This wave packet is associated with the Type I instability mode and the onset of the development of spiral vortices within the boundary layer. As the Reynolds number is increased further to $Re=490$ the whole circumference of the disk becomes occupied by spiral vortices. This is evident from the signal displaying a characteristic frequency over the entire time interval displayed. Increasing the Reynolds number to still higher values soon leads to the breakdown of the spiral vortices and to the final transition to a fully turbulent flow. This is revealed by the velocity signals corresponding to $Re=504$ and $Re=518$ which no longer show clear evidence of the presence of a characteristic frequency. The above description for the development of the velocity signals is consistent with the theory and observations of Lingwood^{11,12} and Wilkinson and Malik²⁶ for the flow over a rigid disk spinning in air. A comparison of our data of Fig. 3(a) with the corresponding signals in Fig. 2 of Jarre *et al.*,²² which were obtained for a disk spinning under water, also reveal good agreement. It can, thus, be concluded that we are able to reproduce the results of previous studies. Consequently, it appears justified to assume that any differences between velocity signals collected over a rigid disk and a compliant disk can be attributed to a changed nature of the flow associated with the different surface properties. To establish this was crucial for the remainder of the data analysis. Results comparable to those presented above for the rigid disk have previously not been documented in the literature for the case of a compliant disk.

The velocity-time traces for the flow over a compliant disc are displayed in Fig. 3(b). The signal for $Re=252$ displays two double-peak disturbances which originated at the roughness element. They were captured by the hot-film probe at times $t \approx 0.075$ s and $t \approx 0.875$ s. The disturbances are spaced 0.8 s apart corresponding to the time of revolution associated with a rotational frequency of $f_D=1.25$ Hz. The reason for the change from a single-peak to a double-peak

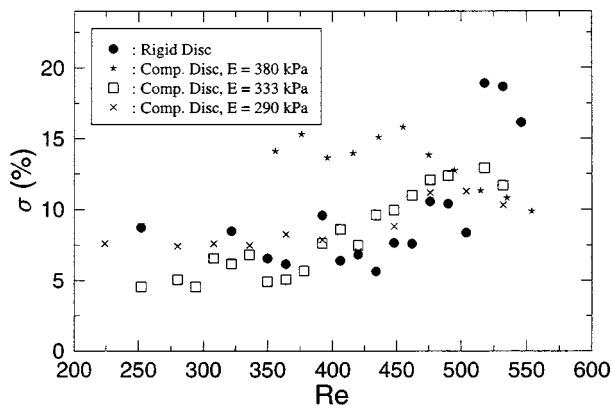


FIG. 4. Comparison of the variation of the turbulence intensity σ of the azimuthal component of the flow velocity with the Reynolds number for rigid and compliant disks ($\Omega=7.85$ rad/s, $\zeta=1.29$).

structure for this particular set of data is not known for certain. It is, of course, virtually impossible to adhere a small roughness element to a relatively soft silicone-rubber surface without otherwise modifying the surface to some extent and the double-peak structure may well reflect such an inadvertent modification. In the interval between the two disturbances the flow velocity is almost constant—apart from a small disturbance at $t=0.24$ s. In contrast to the case for the flow over a rigid disk the disturbance introduced by the roughness element appears to have a larger influence on the boundary-layer flow structure for the compliant wall. Already for the next larger Reynolds number displayed, at $Re=294$, the signal appears to be relatively noisy over the entire time domain. The corresponding signal for the rigid disk at this Reynolds number is still smooth over the entire time interval between the disturbance peaks. As the Reynolds number is increased to $Re=322$ evidence of the presence of vortices appears in the signal and remains visible up to approximately $Re=420$ or $Re=434$. The flow becomes fully turbulent in the Reynolds number range $448 \leq Re \leq 462$.

In summary, then, our experimental results show that flow transition over the compliant disk occurs at a substantially lower Reynolds number than over a rigid disk. It is emphasized that this earlier transition is not a consequence of a larger disturbance of the boundary-layer flow associated with the double-peak structure of the disturbance peak discussed above in the context of Fig. 3(b). When the experiments involving the compliant disk were repeated four months after the date for which the data in Fig. 3(a) and 3(b) were collected the double-peak structure was not observed but transition still occurred at a similarly low Reynolds number.

In order to present some more quantitative remarks concerning the development of the hot-film signals over the rigid and the compliant disk Fig. 4 shows the turbulence intensities σ relating to the flow velocity measurements. Figure 4 displays the variations of turbulence intensity of the azimuthal velocity component with radius at a fixed height $\zeta=1.29$. The values of σ are given in percent with respect to the mean flow velocity measured at the particular radial locations. The figure reveals that the peak turbulence intensity

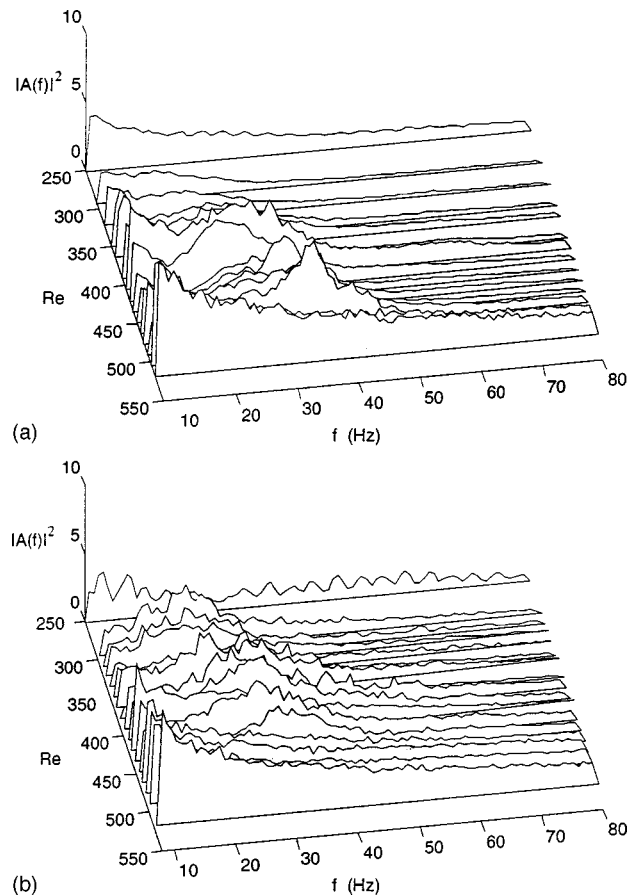


FIG. 5. Three-dimensional view of the evolution of Fourier energy spectra with the Reynolds number. (a) Rigid disk, (b) compliant disk.

in the transition regime between $Re \approx 470$ and $Re \approx 550$ is lower over the compliant disk than over the rigid disk. This effect appears to persist into the fully turbulent regime. This result is consistent with the recent observations made by Choi *et al.*³² in their experimental study of turbulent boundary layers in water flow over similarly fairly stiff, silicone-rubber, compliant walls.

C. Fourier spectra obtained from velocity signals

The qualitative comparison of the velocity–time signals discussed in the preceding section has already shown that for the particular compliant wall used in our experiments the overall effect of compliance resulted in transition at lower Reynolds numbers. Nevertheless, the detailed data analysis presented below will reveal that wall compliance appears to have a stabilizing effect in the frequency range associated with the Type I eigenmode.

Figures 5(a) and 5(b) present the Fourier frequency spectra obtained from analyzing signals of the azimuthal component of the flow velocity over a rigid and a compliant disk, respectively. The figures display the Reynolds number Re and the frequency f of the Fourier modes on the horizontal axes. The vertical axis of each figure represents the energy contained in the Fourier modes in terms of the square of their amplitude $A(f)$. The angular velocity of the disc for which the displayed data were obtained is $\Omega=7.85$ rad/s. The data

were collected at a height $\zeta=1.29$ above the disk surface. For each Reynolds number 60 separate time series of length 1.0 s were recorded with a resolution of 1024 data points per series. The Fourier spectrum for each individual time series was then calculated. The resulting 60 spectra were ensemble averaged to yield one average spectrum for the particular Reynolds number. These averaged spectra are displayed in Figs. 5(a) and 5(b) as a function of their associated Reynolds numbers.

A comparison of our rigid-disk data displayed in Fig. 5(a) with the corresponding Fig. 3 of Jarre *et al.*²¹ (also repeated as Fig. 3 in Jarre *et al.*²²) reveals a good agreement between the experimental data. In both experiments the emergence of a distinct wave packet centered around a frequency of 30–35 Hz is observed. One difference between the present experiment and that of Jarre *et al.*^{21,22} should be emphasized. Jarre *et al.* obtained their data from a disk spinning at a rotational frequency $f_D=1$ Hz, whereas in the present experiment the disk was spinning at $f_D=1.25$ Hz. If the spiral vortices are stationary in the frame of reference of the rotating disk, then the emerging wave packet in Fig. 3 of Jarre *et al.*^{21,22} is centered around a frequency whose value directly relates to the number of structures (spiral vortices) developing in the boundary layer. In the present case the higher rotational frequency f_D needs to be taken into account. Consequently our results indicate the presence of a slightly smaller number of spiral vortices than the Jarre *et al.* data. Our data suggest the presence of between approximately $f/f_D=24$ and 28 spiral vortices. This result is, in fact, in excellent agreement with the results of Malik *et al.*³³ and Wilkinson and Malik.²⁶

Figure 5(b) shows the corresponding power spectra for the compliant disk. Similar to Fig. 5(a) a wave packet centered around a frequency of 30–35 Hz is seen to develop. A detailed comparison of the two spectra requires a quantitative data analysis. This analysis is presented below.

D. Method for construction of neutral curves

From power spectra such as those displayed in Figs. 5(a) and 5(b) associated neutral stability curves for the Type I instability mode can be constructed. In order to obtain these curves we follow the procedure outlined in Jarre *et al.*^{21,22} The procedure is briefly summarized below.

$A(f)$ is the amplitude of the Fourier mode of frequency f of the ensemble-averaged Fourier spectrum associated with a certain Reynolds number. The value $|A(f)|^2$ is proportional to the energy contained in that mode and can, thus, be employed as a measure for the energy. Plotting the logarithm of $|A(f)|^2$ vs Re reveals how the energy carried by a particular mode changes with the Reynolds number. Typical examples of curves obtained in this way are shown for various frequency values of f/f_D , in Figs. 6(a) and 6(b).

The data contained in Fig. 6(a) were obtained from the spectrum of Fig. 5(a) for the flow over the rigid disk. The corresponding growth curves for the spectrum of Fig. 5(b) for the compliant disk are contained in Colley.³⁴ In Sec. III F it will be discussed how changing levels of compliance associated with the aging of the disk material affect the neutral

stability curves. With regard to this we include here in Fig. 6(b) growth data for the flow over the aged compliant disk when the modulus of elasticity has fallen to $E=290$ kPa. The data shown in Figs. 6(a)–6(b) display minima around certain values Re_m . The estimated minima positions are identified in Fig. 6(a) by short vertical lines which intersect the interpolation curves. In Fig. 6(b) the regions judged to contain the minima are identified by the gray-shaded circles superposed on each data set.

For $\text{Re}<\text{Re}_m$ the energy carried by the Fourier mode decreases with an increasing Reynolds number, whereas it increases for $\text{Re}>\text{Re}_m$. The values of the Reynolds number associated with the positions of the minima consequently represent points located on the neutral stability curve. By determining a sufficiently large number of locations of minima as a function of their associated frequencies the neutral stability curve can thus be constructed.

We did not follow the procedure of Jarre *et al.*^{21,22} who determined the values of the Reynolds numbers associated with the minima positions by means of polynomial interpolations of the data. In general our data points display a somewhat larger scatter than those presented in Jarre *et al.*^{21,22} As a result polynomial interpolations of our data yielded, in many cases, values for the critical Reynolds number which evidently did not coincide with the true location of the minimum. As a consequence of this we decided to draw curves through the data points by hand. It is emphasized, however, that this procedure contains no more ambiguity than fitting a polynomial of arbitrarily chosen degree. The estimated largest error involved in determining the position of the minima from our data is of the order of $\Delta\text{Re}=\pm 10$. It is noted that it is, of course, only permissible to construct the neutral stability curve in the way described if the data of all time series are collected in a completely identical format. Hence, the length of all time series must remain constant as well as the number of sampled data points per series. Unless this is ensured the scale on the $|A(f)|^2$ axis representing the energy is changed from one time series to the next. It would then not be permissible to construct a neutral stability curve in the way outlined above.

E. Neutral curve for the type I mode over a rigid disk

Figure 7 shows the neutral stability points determined for the Type I instability for the flow over a rigid disk in comparison to the results of previous authors. The critical Reynolds number is plotted as a function of f/f_D . This ratio corresponds to the quantity β in the notation of Jarre *et al.*²² provided that the disturbances are stationary with respect to the rotating disk. Our data are compared to the experimental results of Jarre *et al.* and to the theoretical prediction of Malik.³⁵ It can be seen that the position of the minimum of the neutral stability curve displayed by our data is in somewhat better agreement with Malik's theoretical prediction than the corresponding experimental results of Jarre *et al.* Malik's theoretical results correspond to stationary disturbances. Consequently our data suggest that at the point of instability, at least, the spiral vortices in the boundary layer of our disk were stationary in the reference frame of the

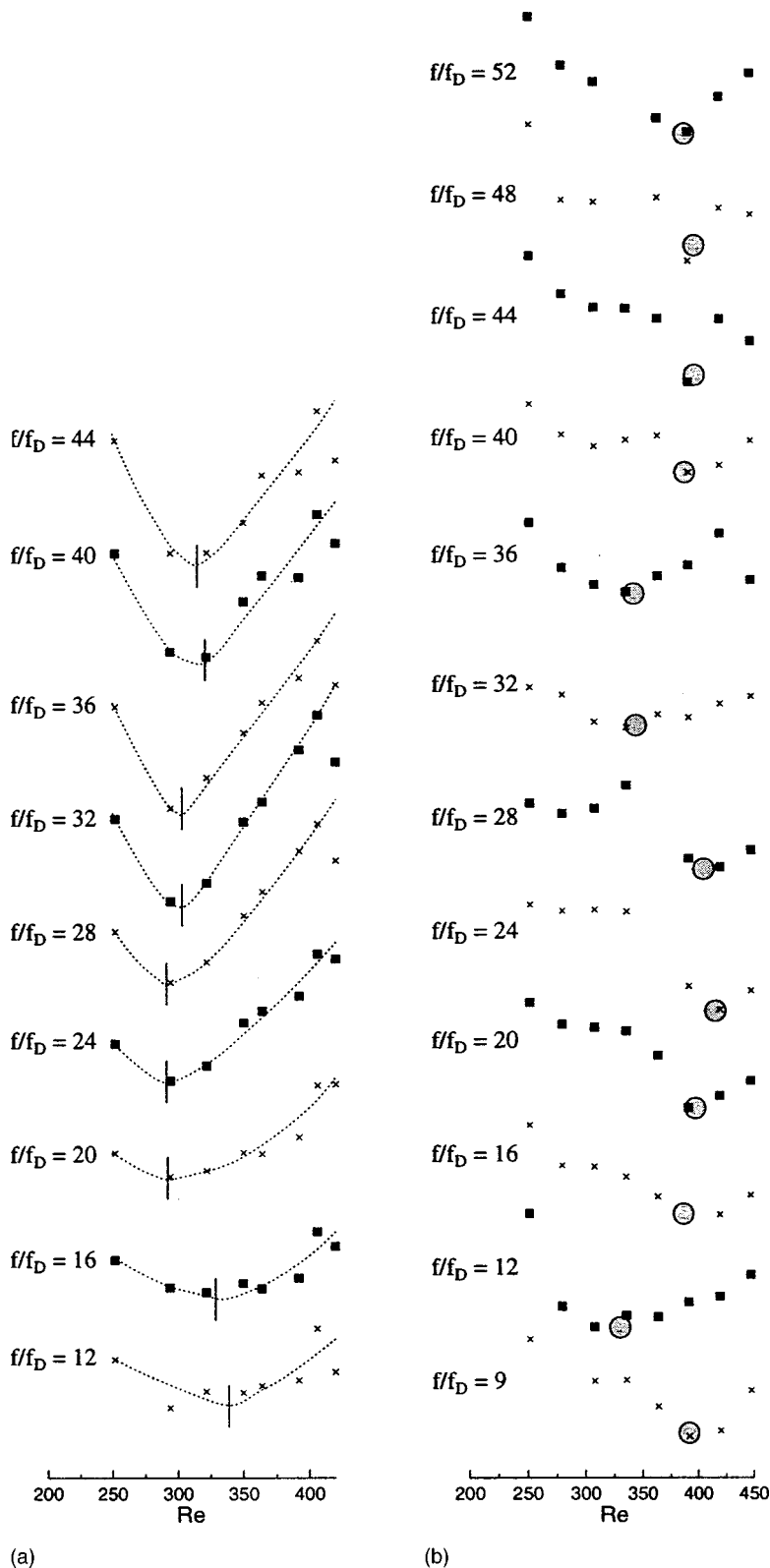


FIG. 6. Total amplification diagrams for various frequencies f/f_D . The displayed data are for (a) rigid disk and (b) compliant disk with a modulus of elasticity of $E = 290$ kPa. The ordinate of each curve corresponds to $\log_{10}(|A(f/f_D)|^2)$. The scale of the ordinate is different in (a) and (b) but it is the same within each series for the different values of f/f_D . The estimated minima positions are identified in (a) by the short vertical lines crossing the interpolation curves. In (b) the estimated region containing the minima is identified by the gray-shaded circles.

rotating disk. Nevertheless, from the experience we have gained throughout the data collection we believe that this result might be fortuitous and that the spiral vortices were not strictly stationary. Evidence for this is provided from ensemble averages of the 60 individual time series collected at each Reynolds number. Such an averaging for a particular Reynolds number yields a mean signal which does not reveal

any evidence of the presence of spiral vortices even when each individual signal does clearly do so. We intend to address to this matter in more detail in the future. However, with respect to the goal of the present study the main significance of Fig. 7 is that it shows that we are able to reproduce the curves of neutral stability determined by other authors with reasonable accuracy. The good agreement of our experi-

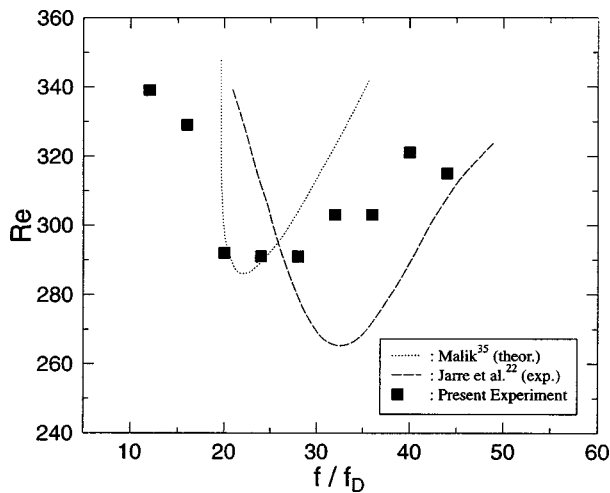


FIG. 7. Comparison of the neutral stability curve obtained from the experimental data with corresponding theoretical and experimental results of other authors.

mental data with the results of Malik³⁵ further indicates that any recirculation of flow disturbances in the enclosed space between the disk and the lid did not lead to significant effects on the neutral stability curve of the Type I mode.

F. Neutral curve for the type I mode over a compliant disk

We will now proceed to the main part of this study and compare the neutral stability curve obtained for the rigid disk with corresponding data obtained for a disk covered with a compliant surface. This comparison is shown in Fig. 8. The figure displays four sets of experimental data. The squares redisplay our data for the rigid-disk case which were already contained in the preceding Fig. 7. Additionally Fig. 8 contains three sets of data for the compliant disk. These three sets were obtained for the flow over the same compliant disk.

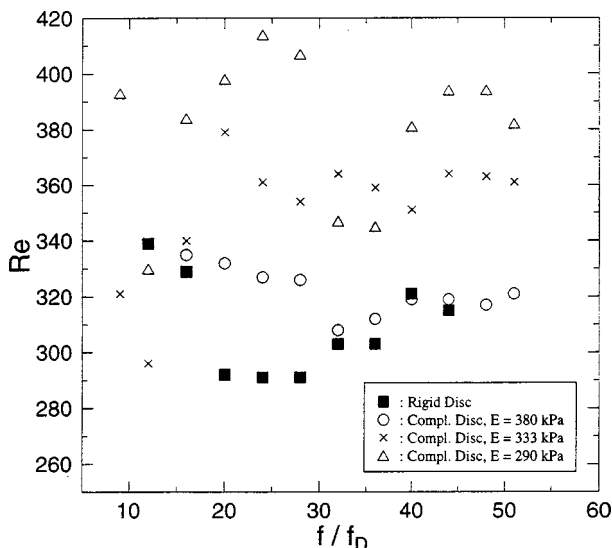


FIG. 8. Comparison of the neutral stability curve obtained for a rigid disk with the corresponding curves obtained for compliant disks. The three data sets for the compliant disk surface were obtained at different instances during the aging process of the coating material.

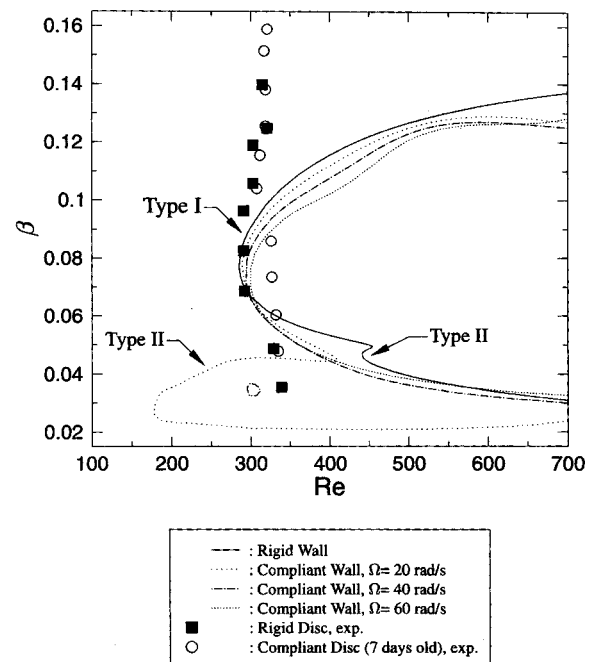


FIG. 9. Neutral stability curve for stationary disturbances over rigid and compliant surfaces. The three curves for different rotational disk speeds Ω correspond to three different levels of effective disk compliance.

The data were, however, collected at different times after manufacturing the coating as was described in Sec. II and they correspond, consequently, to different values of the modulus of elasticity. The experimental data from which the neutral curve associated with the lowest value $E = 290$ kPa of the modulus of elasticity was obtained are shown in Fig. 6(b). As Fig. 6(b) reveals it is in some cases not an easy matter to unambiguously locate the minima position Re_m for the compliant-disk data. Nevertheless, the data analysis has shown that there is a clear trend for the minima positions of all compliant cases studied being located at higher Reynolds numbers than the corresponding positions for the rigid disk. This trend is reflected in Fig. 8 where all data for the compliant disk are clearly shifted towards higher Reynolds numbers in comparison to the rigid-disk results. This observation suggests, first, that effects on the Type I instability depend on the age and external factors affecting the compliant material. Second, as the Reynolds number at any value of f/f_D is consistently higher for the compliant disk than for the rigid disk our results imply that wall compliance has a stabilizing effect on the Type I instability mode. This is one of the main results of this paper.

IV. COMPARISON OF EXPERIMENTAL DATA WITH THEORY

The theory for the effect of wall compliance on the boundary-layer stability over the rotating disk is presented in Cooper and Carpenter.^{2,13} Cooper and Carpenter give a detailed description of their theoretical and numerical methods and this need not be repeated here. Figure 9 displays their computed curves of neutral stability for stationary disturbances of Type I and Type II over rigid and compliant

boundaries in comparison to some of the experimental data of the present experiment. The two experimental data sets shown in the figure correspond to the two sets referred to as ‘‘Rigid Disk’’ and ‘‘Compliant Disk, $E=380$ kPa’’ of Fig. 8. The abscissa of Fig. 9 shows the critical Reynolds number. The ordinate shows the azimuthal disturbance wave number β which is equal to (Malik *et al.*³³)

$$\beta = \frac{n}{\text{Re}}. \quad (8)$$

In Eq. (8) n is the number of vortices filling the circumference of the disk at the particular radial location associated with the value of the Reynolds number. For stationary disturbances the value of n corresponds to the ratio f/f_D introduced during the discussion of Fig. 8.

For the comparison of the experimental and the theoretical results we will initially follow previous authors and assume that the roughness element used in our experiments generated predominantly stationary disturbances. What does our theory suggest the effect of wall compliance should be on such stationary disturbances? The theoretical predictions are illustrated by considering Fig. 9. For the calculations it was assumed that the compliant wall is a homogeneous viscoelastic layer of infinite depth. The modulus of elasticity was assumed to have a fixed value of $E=3$ kPa. It is explained in Cooper and Carpenter² that for such a constant modulus of elasticity the effective level of compliance increases with an increasing rotational speed of the disk. (Also the viscoelastic damping coefficient is set to zero but, in any case, has little effect on such stationary disturbances.) Consequently Fig. 9 shows that increasing the level of wall compliance stabilizes the Type I instability as is evidenced by the rise in the critical Reynolds number for the higher rotational speeds of the disk. For the Type II instability the effect of wall compliance is more complex. The Type II mode has a much higher critical Reynolds number of about 440 than the Type I mode for the case of the rigid wall. Compliant, but relatively stiff, surfaces ($\Omega=20$ rad/s) are destabilizing and the critical Reynolds number is significantly reduced to about 175 at $\beta=0.03$. For relatively soft surfaces (high disk speeds), however, compliance has a stabilizing effect. Hence, our theory appears to agree qualitatively with the experimental results presented in Fig. 8. The critical Reynolds number corresponding to the wave-number range associated with the Type I instability is indeed higher for the compliant disc than for the rigid one, for both, the experiment as well as for the numerical data. Further, the experimental data discussed in Sec. III B showed that the compliant coating has destabilized the boundary-layer flow; the overall transition to turbulence did occur at a lower critical Reynolds number for the compliant disk than for the rigid disk. With regard to the conclusions obtained from the discussion of Fig. 9 this result could, consequently, be attributed to the destabilizing effect of wall compliance in the range of lower wave numbers associated with the Type II mode. Nevertheless, in an important respect the theory is not corroborated by the experimental data. The compliant walls used in the experiments have elastic moduli ($290 \text{ kPa} \leq E \leq 390 \text{ kPa}$) which are two orders of magnitude

higher than the value assumed for the computations ($E=3$ kPa). For relatively stiff walls such as those actually used in the experiments our computations yielded neutral stability curves and other stability characteristics which are indistinguishable from those for the rigid wall.

This lack of quantitative corroboration between theory and experiment suggests that other explanations for the effects of wall compliance on transition might have to be considered. One approach to this problem is to question our initial assumptions that it is stationary disturbances which are dominant in the boundary layer. From theory it is indeed known that traveling disturbances are less stable than their stationary counterparts.^{36,37} This effect is particularly pronounced for the Type II instabilities. Even for the rigid wall the critical Reynolds number for the most unstable traveling Type II disturbance is significantly lower than that for the Type I, whereas for stationary disturbances the position is reversed. The most outstanding phenomenon associated with traveling disturbances is, however, the absolute instability discovered by Lingwood^{11,12} in her theoretical and experimental study. She advanced convincing arguments for this absolute instability being the actual route to transition for the rotating-disk boundary layer.

As in most of the previous studies, our measurements were carried out with a single fixed probe. Consequently it is not possible to obtain direct experimental evidence of traveling disturbances from our measurements. However, Jarre *et al.*²² have carried out experiments similar to ours over a rigid disk. They conducted experiments during which they measured with two hot-film probes simultaneously. Their results indicate that small roughness elements generate traveling, rather than stationary, disturbances. Accordingly, we may well conclude that traveling disturbances were probably dominant in our experiments.

Our theory identifies two potentially powerful routes to transition. On the one hand, as shown by Lingwood, there is the absolute instability. However, the theory due to Cooper and Carpenter¹³ shows quite emphatically that even a very small level of compliance brings about a substantial rise in the critical Reynolds number for the onset of absolute instability. Accordingly, absolute instability would appear to be ruled out as the route to transition in our experiments. The other possible mechanism identified by Cooper and Carpenter² (and also noted by Lingwood¹¹ in the case of the rigid wall) is the occurrence of modal coalescence between the Type I and Type II eigenmodes. This does not lead to absolute instability, but rather to localized algebraic growth which occurs at Reynolds numbers which are subcritical with respect to the Type I mode. In the case of the rigid wall the coalescence first occurs at fairly high Reynolds numbers and the algebraic growth is dominated by other effects like the absolute instability. However, for compliant walls the algebraic growth occurs at much lower Reynolds numbers. Accordingly this might be a much more significant route to transition especially in a relatively high-noise flow environment. Whether or not such algebraic growth is responsible for transition in our experiments is impossible to determine at this stage and must await further experimental study.

Finally, one other significant observation to emerge from our study concerns the Lingwood absolute instability. A factor motivating Lingwood's study was the observation due to Gaster (personal communication contained in Lingwood¹¹) that flow visualizations of the rotating disk flow reveal that the onset of transition occurs always at a well-defined radius, i.e., abruptly and axisymmetrically. Lingwood¹¹ also points out that in all previously documented experimental studies of transition over a rotating disk the actual transition occurred within a very narrow Reynolds number interval located at $Re \approx 513 \pm 15$. This is quite unlike laminar-turbulent transition in boundary layers when convective instabilities are known to be involved, e.g., the growth of Tollmien-Schlichting waves in the flat-plate boundary layer or transition in pipe flows. In such cases the transitional Reynolds number varies greatly with the disturbance level and/or the background noise level. Our rigid-disk experiment corroborates previous experimental studies in that the transitional Reynolds number lies between 504 and 518. On the other hand we have observed that for the compliant disk transition occurs at a much lower Reynolds number in the range between 448 and 462. To the best of our knowledge this is the first documented case where the transitional Reynolds number for the rotating disk falls below the narrow range cited above. This might suggest that for the compliant disk the transition mechanism is not the absolute instability. Whether or not the transition point is sensitive to the size of the initial disturbance or to the noise in the environment is not known at present and this question will have to be addressed at a later stage.

V. CONCLUSION

We have presented an experimental study concerned with the laminar-turbulent transition of the boundary-layer flow developing over a rotating disk immersed under water. The main aim of the study was to investigate the effect of wall compliance on the physics of the transition process. We have experimentally determined the neutral stability curve for the Type I instability mode for the rigid and the compliant disk. This appears to be the first time that such experimental data have been presented for the case of the compliant disk. Our results for the flow over the rigid disk essentially corroborate the results obtained by other authors in the past. The main results and conclusions of our study are as follows. Our measurements have shown that the turbulence levels in the transition regime over a compliant disk are significantly lower than the corresponding levels for the rigid disk. Our data analysis has revealed that compliance appears to have a stabilizing effect on the Type I instability mode. The overall effect of compliance for the particular elastic material used to coat the disk was, nevertheless, destabilizing and resulted in a transition at lower Reynolds numbers. Both these experimental observations are in qualitative agreement with our associated numerical computations. A quantitative comparison of experimental and theoretical data was, however, less favorable. The numerical data based on our theoretical considerations indicate that for the level of compliance used in our experiments there should

have been no discernible difference in the stability characteristics from the rigid disk. The transition over the compliant disk was observed to occur at Reynolds numbers which are substantially lower than the corresponding values for the rigid disk. The discussion of this observation has led us to speculate that transition over the compliant disk results from a convective-instability mechanism. This is in contrast to the absolute-instability mechanism which has recently been proposed by Lingwood^{11,12} as the dominant route to transition for the flow over a rigid disk.

Our study has revealed that the use of fairly stiff compliant walls has a surprisingly strong effect on laminar-turbulent transition in the rotating-disk boundary layer. There is currently no theoretical explanation for this and further experimental and theoretical work is required to elucidate the physical mechanisms involved.

ACKNOWLEDGMENTS

The work described in this paper was supported by research grants from the Engineering and Physical Sciences Research Council (EPSRC) and the Marine Technology Directorate (MTD).

- ¹H. L. Reed and W. S. Saric, "Stability of three-dimensional boundary layers," *Annu. Rev. Fluid Mech.* **21**, 235 (1989).
- ²A. J. Cooper and P. W. Carpenter, "The stability of the rotating-disk boundary-layer flow over a compliant wall. 1. Type I and Type II instabilities," *J. Fluid Mech.* **350**, 231 (1997).
- ³Th. von Kármán, "Über laminare und turbulente Reibung," *Z. Angew. Math. Mech.* **1**, 233 (1921).
- ⁴N. Gregory, J. T. Stuart, and W. S. Walker, "On the stability of three-dimensional boundary layers with application to the flow due to a rotating disk," *Philos. Trans. R. Soc. London, Ser. A* **248**, 155 (1955).
- ⁵M. O. Kramer, "Boundary layer stabilization by distributed damping," *J. Am. Soc. Naval Eng.* **72**, 25 (1960).
- ⁶T. B. Benjamin, "Effects of a flexible boundary on hydrodynamic stability," *J. Fluid Mech.* **9**, 513 (1960).
- ⁷M. T. Landahl, "On the stability of a laminar incompressible boundary layer over a flexible surface," *J. Fluid Mech.* **13**, 609 (1962).
- ⁸P. W. Carpenter and A. D. Garrad, "The hydrodynamic stability of flow over Kramer-type compliant surfaces. Part 1. Tollmien-Schlichting instabilities," *J. Fluid Mech.* **155**, 465 (1985).
- ⁹M. Gaster 1987, "Is the dolphin a red herring?" in *Proceedings of the IUTAM Symposium on Turbulence Management and Relaminarization*, Bangalore, India, edited by H. W. Liepmann and R. Narasimha (Springer, Berlin, 1987), pp. 285-304.
- ¹⁰A. D. Lucey and P. W. Carpenter, "Boundary-layer instability over compliant walls: Comparison between theory and experiment," *Phys. Fluids* **7**, 2355 (1995).
- ¹¹R. J. Lingwood, "Absolute instability of the boundary layer on a rotating disk," *J. Fluid Mech.* **299**, 17 (1995).
- ¹²R. J. Lingwood, "An experimental study of absolute instability of the rotating-disk boundary-layer flow," *J. Fluid Mech.* **314**, 373 (1996).
- ¹³A. J. Cooper and P. W. Carpenter, "The stability of the rotating-disk boundary-layer flow over a compliant wall. 2. Absolute Instability," *J. Fluid Mech.* **350**, 261 (1997).
- ¹⁴R. J. Hansen and D. L. Hunston, "An experimental study of turbulent flows over compliant surfaces," *J. Sound Vib.* **34**, 297 (1974).
- ¹⁵R. J. Hansen and D. L. Hunston, "Further observations on flow-generated surface waves in compliant surfaces," *J. Sound Vib.* **46**, 593 (1976).
- ¹⁶R. J. Hansen and D. L. Hunston, "Fluid-property effects on flow-generated waves on a compliant surface," *J. Fluid Mech.* **133**, 161 (1983).
- ¹⁷K. H. Chung, "Composite compliant coatings for drag reduction utilizing low modulus high damping silicone rubber," Ph.D. thesis, Massachusetts Institute of Technology, 1985.
- ¹⁸E. R. Fitzgerald and J. W. Fitzgerald, "Blubber and compliant coatings for drag reduction in fluids. V. Driving point shear impedance measurements

- on compliant surfaces," in Proceedings of the International Symposium on Seawater Drag Reduction, Newport, Rhode Island, edited by J. C. S. Meng, 1998, p. 211 (unpublished).
- ¹⁹J. W. Fitzgerald, J. E. Martin, and E. F. Modert, "Blubber and compliant coatings for drag reduction in fluids. VI. Rotating disk apparatus for drag measurement on compliant layers," in Proceedings of the International Symposium on Seawater Drag Reduction, Newport, Rhode Island, edited by J. C. S. Meng, 1998, p. 215 (unpublished).
- ²⁰J. M. Owen and R. H. Rogers, "Flow and Heat Transfer in Rotating-Disk Systems (Research Studies, Taunton, Somerset, England, 1989), Vol. 1, p. 47.
- ²¹S. Jarre, P. Le Gal, and M. P. Chauve, "Experimental analysis of the instability of the boundary layer over a rotating disk," *Europhys. Lett.* **14**, 649 (1991).
- ²²S. Jarre, P. Le Gal, and M. P. Chauve, "Experimental study of rotating disk instability. I. Natural flow," *Phys. Fluids* **8**, 496 (1996).
- ²³S. Jarre, P. Le Gal, and M. P. Chauve, "Experimental study of rotating disk instability. II. Forced flow," *Phys. Fluids* **8**, 2985 (1996).
- ²⁴M. Wimmer, "Viscous flows and instabilities near rotating bodies," *Prog. Aerosp. Sci.* **25**, 43 (1988).
- ²⁵H. H. Bruun, *Hot-Wire Anemometry* (Oxford University Press, Oxford, 1995), pp. 71ff and 134–135.
- ²⁶S. P. Wilkinson and M. R. Malik, "Stability experiments in the flow over a rotating disk," *AIAA J.* **23**, 588 (1985).
- ²⁷T. R. Thomas, C. F. Holmes, M. T. McAdams, and J. C. Bernard, "Surface features influencing the effectiveness of lip seals: A pattern recognition approach," SME Paper No. IQ 75-128, 1975.
- ²⁸*Principles of Tribology*, edited by J. Halling (MacMillan, London, 1975), p. 60.
- ²⁹G. K. Batchelor, "Note on a class of solutions of the Navier–Stokes equations representing steady rotationally-symmetric flow," *Q. J. Mech. Appl. Math.* **4**, 29 (1951).
- ³⁰M. H. Rogers and G. N. Lance, "The rotationally symmetric flow of a viscous fluid in the presence of an infinite rotating disk," *J. Fluid Mech.* **7**, 617 (1960).
- ³¹D. Dijkstra and G. J. F. van Heijst, "The flow between two finite rotating disks enclosed by a cylinder," *J. Fluid Mech.* **128**, 123 (1983).
- ³²K.-S. Choi, X. Yang, B. R. Clayton, E. J. Glover, M. Atlar, B. N. Semenov, and V. M. Kulik, "Turbulent drag reduction using compliant surfaces," *Proc. R. Soc. London, Ser. A* **453**, 2229 (1997).
- ³³M. R. Malik, S. P. Wilkinson, and S. A. Orszag, "Instability and transition in rotating disk flow," *AIAA J.* **19**, 1131 (1981).
- ³⁴A. J. Colley, "An experimental investigation of the flow in the boundary layer above a rotating disk, with compliant characteristics, in water," Ph.D. dissertation, Department of Engineering, University of Warwick, Coventry, England, 1997.
- ³⁵M. R. Malik, "The neutral curve for stationary disturbances in a rotating-disk flow," *J. Fluid Mech.* **164**, 275 (1986).
- ³⁶L. M. Mack, "The wave pattern produced by a point source on a rotating disk," AIAA Paper No. 85-0490, 1985.
- ³⁷P. Balakumar and M. R. Malik, "Traveling disturbances in rotating-disk flow," *Theor. Comput. Fluid Dyn.* **2**, 125 (1990).